Euro PM2018 congress, October, Bilbao - Spain

Heat Treatment Optimization via Thermo-Physical Characterization of AlSi7Mg and AlSi10Mg Manufactured by Laser Powder Bed Fusion (LPBF).

Van Cauwenbergh Pierre[1], Beckers Anthony[1], Thijs Lore[1], Van Hooreweder Brecht[2], Vanmeensel Kim[2]

[1] 3D Systems Leuven
Grauwmeer 14, Leuven 3001, Belgium
Pierre.vancauwenbergh@3dsystems.com, Anthony.beckers@3dsystems.com, Lore.thijs@3dsystems.com
[2] KU Leuven
Celestijnenlaan 300 - box 2420, Leuven 3001, Belgium
Brecht.vanhooreweder@kuleuven.be
Kasteelpark Arenberg 44 - box 2450, Leuven 3001, Belgium
Kim.vanmeensel@kuleuven.be

Abstract The current paper aims at unraveling the threefold interrelationship between process, microstructure and properties of two materials, AlSi7Mg and AlSi10Mg, processed by laser powder bed fusion (LPBF) on a 3D Systems ProX® DMP 320, and subsequently heat treated under different conditions in argon atmosphere. Three thermo-physical characterization techniques were employed to monitor microstructural and concomitant mechanical property changes during heat treatment of LPBF processed Al-Si-Mg based alloys. The evolution of dissolved Si in the FCC Al matrix was monitored by electrical resistivity (ER) measurements, precipitation reactions were monitored by combining differential scanning calorimetry (DSC) with elastic property and damping measurements using the impulse excitation technique (IET). The evolution of the microstructure upon heat treatment was linked to characteristic phenomena captured by each of the three thermo-physical characterization techniques. Finally, the evolution of internal and residual stresses of both processed alloys upon heat treatment was monitored via the cantilever method.

Key words: Laser Powder Bed Fusion, AlSi7Mg, AlSi10Mg, Heat Treatment, Thermo-Physical Characterization

INTRODUCTION

Laser Powder Bed Fusion (LPBF) is an additive manufacturing process that uses 3D Computer Aided Design (CAD) data to build an object layer-by-layer, and is also known as Direct Metal Printing (DMP). The process consists of a high-energy intensity laser beam that scans over the powder bed and selectively fuses particles together according to the profile of that object [1], [2], [3]. Yet, the layer-by-layer LPBF process induces an intense cyclic heating and cooling pattern in the material, which results in unique solidification conditions and an ultrafine metastable microstructure [1], [2], [4]. In addition, very high cooling rates (10^4-10^6 °C/s) along the building direction are observed and lead to severe accumulation of residual stresses during the built [3]. This makes that the microstructure of LPBF parts differs fundamentally from conventionally manufactured parts.

The state-of-the-art production of LPBF parts shows that great progress has been made concerning the optimization of the LPBF process itself, with the aim of acquiring consistently high quality and fully dense parts. After the built, the parts commonly undergo a heat treatment in order to relieve residual stresses or homogenize the LPBF microstructure, resulting in more isotropic and consistent mechanical properties [5]**.** Therefore, heat treatments are often just as critical as the LPBF build process itself, in order to assure high quality parts**.** However, only few efforts have been undertaken to optimize the heat treatments for LBPF lightweight Al alloys (e.g. AlSi7Mg, AlSi10Mg). The Al-Si-Mg alloy is a precipitation hardenable alloy for which a T6 (Solution annealing + Ageing) heat treatment has been optimized for conventionally cast Al-Si-Mg alloys. This conventional T6 heat treatment is, however, often applied on LBPF Al-Si-Mg alloys with an intrinsically different microstructure compared to conventionally cast parts [3], [5], [6]. Therefore, the T6 heat treated LPBF parts often exhibit inferior properties compared to conventionally cast and T6 heat treated Al-Si-Mg alloy [3]. During the T6 solution annealing step, excessive grain coarsening of the ultrafine LPBF microstructure occurs. Consequently, the high strength properties, obtained from the unique LPBF Al-Si-Mg microstructure, are annihilated [3], [5], [6]. As such, this example marks the need for heat treatments to be designed and tailored specifically for LPBF Al-Si-Mg alloys. In order to tailor post-process heat treatments for LPBF Al-Si-Mg alloys (AlSi7Mg, AlSi10Mg), a detailed thermo-physical characterization of LPBF Al-Si-Mg alloys during heat treatment

was carried out. The goal of this investigation is to link microstructural changes to thermo-physical phenomena that can be captured and monitored throughout the heat treatment procedure.

MATERIAL AND METHODS

The work comprises the study of two Al-Si-Mg alloys, i.e. AlSi7Mg and AlSi10Mg. Both powders have an average particle size of about 40µm. The chemical composition of these alloys are listed in Table 1. The change in silicon and magnesium content is the most important chemical difference that distinguishes AlSi7Mg from AlSi10Mg. Vertical test samples of AlSi7Mg and AlSi10Mg were manufactured via LPBF on a 3D Systems ProX® DMP 320 with each the default parameter sets (set 1, set 2) as provided by 3D Systems ProX DMP 320 Laserform® AlSi7Mg(A) and Laserform® AlSi10Mg(A). The density of the as-printed AlSi7Mg and as-printed AlSi10Mg were above 99.9%. The density was measured with pixel count, and is based on 10 optical micrographs with magnification 5x. The LPBF AlSi7Mg and LPBF AlSi10Mg were tested in as-printed condition as well as after several heat treatment conditions, as listed in Table 2.

Table 1: Chemical composition of LPBF AlSi7Mg and LPBF AlSi10Mg.

Material	Al	Si	Mg	Fe	Cu	Mn	Ni	Zn	Pb	Sn	Ti
Laserform® AlSi7Mg (A)	Bal.	6.5-7.5	0.45-0.7	≤0.19	≤0.05	≤0.10	-	≤0.07	-	-	≤0.25
Laserform® AlSi10Mg (A)	Bal.	9-11	0.2-0.45	≤0.55	≤0.10	≤0.35	≤0.05	≤0.10	≤0.05	≤0.05	≤0.15

Table 2: Overview of the sample conditions.

Sample reference	**Condition**	**Material**
As-built	LBPF As-built	AlSi7Mg / AlSi10Mg
DA	Direct Ageing 170°C during 6h	AlSi7Mg / AlSi10Mg
SR1	Stress Relief 270°C during 2h	AlSi7Mg / AlSi10Mg
SR2	Stress Relief 300°C during 2h	AlSi7Mg / AlSi10Mg

Thermo-physical characterization for both LPBF AlSi7Mg and LPBF AlSi10Mg was performed in this study through various characterization techniques. The electrical resistivity (ER) of Al-Si-Mg test specimens (40x10x3mm³) was determined using a four-point contact technique on a Burster Resistomat type 2302 with a current of 3A and a resistance of 2m.Ω. Differential Scanning Calorimetry (DSC) analysis was performed on a TA Instruments DSC Q2000. The thermal cycles were performed between 20-550°C with a heating and cooling rate of 20°C/min under argon atmosphere. The Impuls Excitation Technique (IET) test was performed on AlSi10Mg with an IMCE RFDA HTVP 1750 device. The test specimen (60x10x3mm³) underwent a thermal cycle between 20-550°C at a heating rate of 5°C/min. Sample preparation was done for microstructural analysis. The Al-Si-Mg samples were grinded with SiC grinding paper from grit 320 to 4000, followed by polishing with diamond suspension of 3µm and 1µm. The samples were etched during 12 seconds with 0.5 vol% HF. The microstructure was observed with a Philips Scanning Electron Microscopy (SEM) XL30 FEG under the conditions: SE, WD 10mm, 5kV, spotsize 3, and magnification 5000x. Tensile testing was done on a Shimadzu AG-X Plus with vertical round near net shaped tensile bars, with test specimen dimension (type 4) and test conditions according to ASTM E8M. Residual stress measurements were performed via the cantilver method. The cantilever shaped test specimens contained a cantilever beam thickness of 1.0mm.

RESULTS AND DISCUSSION

I. Thermo-Physical Characterization

a) Electrical Resistivity

Due to the rapid solidification conditions that are inherent from the LPBF process, the Al-Si-Mg alloy composition deviates from its equilibrium state. Alloying elements, such as Si and Mg, are supersaturated in the Al matrix. Elements in solid solution disturb the lattice structure of the Al matrix. Hence, the lattice disorder as well as the change in the quantum mechanical energy state result in an increase of the electrical resistivity of the material [7]. To estimate the extent of Si supersaturation in the Al matrix, the electrical resistivity of AlSi7Mg and AlSi10Mg was measured for different conditions. The estimation relies on a relation, given by *Tang* [8], who relates the quantitative effect of the dissolved Si content on the electrical resistivity of the Al-Si-Mg alloy. Yet, the verification of the estimated dissolved Si content from *Tang*'s relation was not part of the current work and will be further investigated. In addition, it is important to note that the effect of the dissolved Mg content and the Mg_2Si precipitates is neglected. Figure 1 shows the evolution of the estimated Si content in solid solution for AlSi7Mg and

AlSi10Mg with LPBF parameter sets (set 1, set 2), in as-built and heat treated condition. Mind that the electrical resistivity measurements were converted to electrical conductivity values (%IACS) and plotted in the graph. For both LPBF as-built condition of AlSi7Mg and AlSi10Mg, the dissolved Si content in the Al matrix (2.0-2.7 wt%) exceeds the Si solubility at the eutectic temperature (1.65 wt%). Indeed, these results confirm that the rapid cooling (10^4-10^6 °C/s) induces a supersaturation of the Al-Si-Mg alloy. Consequently, it can be concluded that the solution annealing and quenching step from the T6 heat treatment have become redundant or even harmful for the mechanical properties due to excessive grain coarsening of LPBF Al-Si-Mg. Upon heat treatment, the degree of supersaturation is drastically reduced through the precipitation of Si and Mg_2Si. A partial overlap of the electrical conductivity values for the conditions SR1 and SR2 is observed and may indicate that the remaining Si content in solid solution reaches an equilibrium state. Considering this, the nucleation of Si containing phases decays drastically. For all conditions, AlSi10Mg shows consistently lower conductivity values compared to AlSi7Mg. This observation cannot be explained by a difference in supersaturation, as this would lead to a convergence of the electrical conductivity upon heat treatment. The difference in electrical conductivity may find its reason in the different Si and Mg content between AlSi7Mg and AlSi10Mg. Yet, the Mg content was not taken into account in *Tang*'s relation.

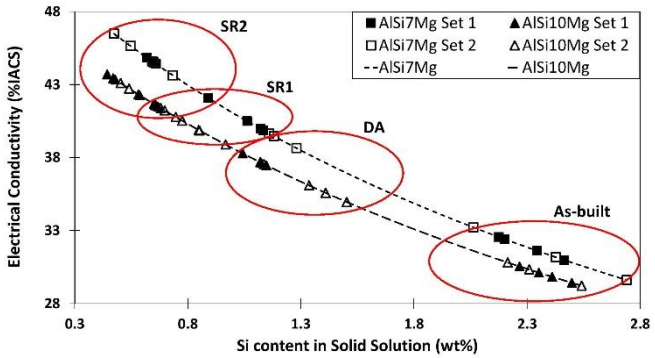

Figure 1: Electrical conductivity values of LPBF AlSi7Mg and AlSi10Mg are plotted as function of the estimated dissolved silicon content in the Al matrix. The graph includes different conditions: As-built, Direct Ageing (DA), Stress Relief (SR1 and SR2), and different laser parameter sets (set 1, set 2).

b) Differential Scanning Calorimetry

The microstructural evolution of LPBF AlSi7Mg and AlSi10Mg upon heat treatment was monitored via Differential Scanning Calorimetry (DSC). Figure 2 shows the specific heat flux curves for the as-built LPBF AlSi7Mg and AlSi10Mg. Upon heating, two distinct first order exothermic reaction peaks occur in both materials. Literature lacks a consensus on the interpretation of these reaction peaks. *Marola et al.* [9] claims that the first peak (160-250°C) is attributed to the precipitation of Si, while the second peak (280-340°C) indicates the precipitation of Mg_2Si. Yet, *Fiocchi et al.* [10] links the first peak to the precipitation of Mg_2Si and the second peak to the diffusional processes of Si. The disappearance of these reaction peaks for repeated DSC cycles confirms that both reactions are driven by the supersaturated condition of the Al matrix. Upon further heating, the thermodynamic equilibrium of the Al-Si-Mg alloy evolves due to the increasing solubility of Si in the Al matrix, from 0.16 wt% to 1.65 wt% between 300°C and 557°C, as shown in the phase diagram in Figure 2 c). Thus, partial dissolution of the precipitated Si and Mg_2Si phases may occur.

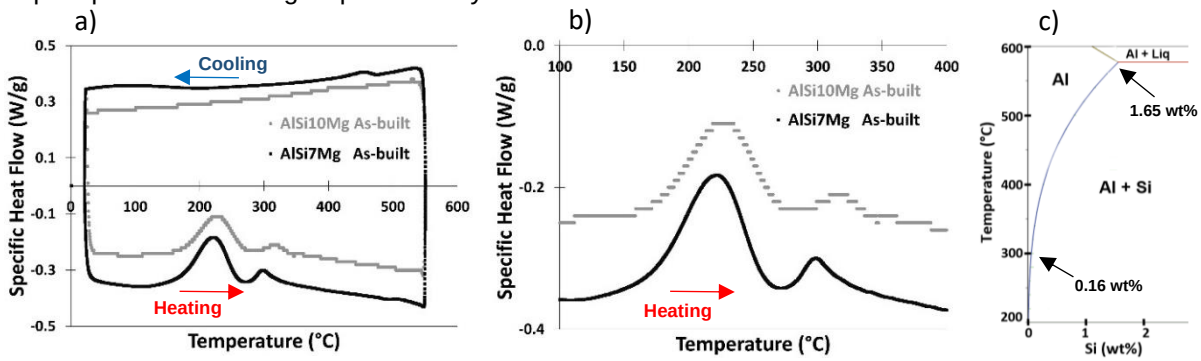

Figure 2: a) DSC curves of AlSi7Mg and AlSi10Mg (LPBF as-built) for the complete thermal cycle, b) detail of the DSC curve with the two first order exothermic reaction peaks, c) Al-Si phase diagram, showing the Si solubility in Al.

c) Impulse Excitation Technique

The Impulse Excitation Technique (IET) allows to monitor the elastic and damping properties and can be used to study lattice defects such as porosities and dislocation movement as well as microstructural evolution through phase transformations, or precipitation and diffusion mechanisms. Therefore, the evolution of the elastic properties of the LPBF AlSi10Mg was measured via in-situ IET (temperature dependent) and ex-situ IET (room temperature), with the aim to link this evolution with the microstructural evolution of the Al-Si-Mg alloy upon thermal post-processing. Figure 3 a) shows the evolution of the Young's modulus of LPBF as-built AlSi10Mg. Within 20-150°C, a linear decay of the Young's modulus is observed, as the material softens with increasing temperature. However, at 150°C the materials behavior starts to deviate from that trend and an increase in the Young's modulus is observed. Once the temperature reaches 220°C, the slope of the increasing Young's modulus starts to decline again. Upon cooling, the Young's modulus linearly increases again till room temperature and indicates that an irreversible material evolution has taken place during the heating cycle. The sudden increase of the Young's Modulus between 150-220°C may be related to the precipitation of Si or Mg2Si from the supersaturated Al matrix. The net increase of the Young's modulus through the IET cycle amounts to 3 GPa. Considering this net increase of 3 GPa, along with a rule of mixture and the Young's modulus of Si (130 GPa), the volume fraction of Si precipitation can be estimated to 2.3%. Whereas, the maximum volume fraction of Mg_2Si that can precipitate (0.57%) together with the Young's Modulus of Mg_2Si (117 GPa), cannot explain the net increase of 3 GPa. Yet, it is important to note that the Young's modulus does also depend on other features such as the dislocation density, crystallographic texture and grain boundary surface area. Thus, the fraction of precipitated Si calculated from the rule of mixture, may be an overestimation. The Young's moduli of LPBF AlSi7Mg and AlSi10Mg for the as-built and heat treated conditions are shown in Figure 3b). The evolution of the Young's modulus seems to give a better correlation with the degree of supersaturation of Si, than with the residual stress state. However, these correlations with the Young's modulus should be further investigated.

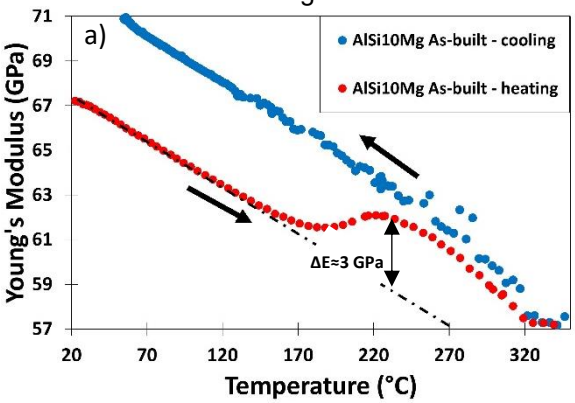

b)

E-modulus (GPa)	AlSi7Mg	AlSi10Mg
As-built	71.1	71.6
DA	74.0	74.4
SR1	75.9	73.9
SR2	75.7	73.2

Figure 3: a) Evolution of the Young's modulus of LPBF AlSi10Mg with temperature via in-situ IET (high temperature). b) Young's modulus of AlSi7Mg and AlSi10Mg for different conditions, measured via ex-situ IET (room temperature).

II. Microstructure

The rapid solidification conditions during the LPBF process result in an ultrafine, submicrometer sized cellular microstructure consisting of supersaturated primary Al cells, surrounded by an nanometer sized fibrous eutectic Si network at the cell boundaries, and is in agreement with the observations made by other researchers [9], [11]–[13]. The as-printed microstructure results from the solidification mechanism where Si is expelled from the Al liquid phase at the solidification front towards the cell boundaries, thus forming the inter-cellular eutectic Si phase. Yet, the fast cooling rates (10^4-10^6 °C/s) causes the primary Al cells to be supersaturated with Si. The degree of Si supersaturation in the primary Al cells as well as the morphology of the Al-Si phase can be modified by changing the laser parameter set [11]. The morphology and size of the eutectic Si network are important factors affecting the mechanical properties [11]–[13]. Although LPBF AlSi7Mg and AlSi10Mg show a similar as-printed microstructure, their microstructural evolution upon heat treatment differs, as seen in Figure 4.

After DA, very fine Si precipitates nucleate in the primary Al cells. As Mg_2Si precipitates are too small to be observed with SEM, it is unclear whether Mg_2Si has precipitated too. Therefore, further investigation with TEM is required to study the size, distribution and morphology of the Mg_2Si precipitates for different heat treatment conditions. Upon SR1, growth of the fine intra-cellular Si precipitates occurs in the primary Al cells, while at the same time, spheroidization of the inter-cellular eutectic Si network occurs. Thus, the microstructure evolves in a fine distribution of spherical Si particles in the Al matrix. At this point, a microstructural difference between AlSi7Mg and AlSi10Mg is noticed. A hypothesis is

suggested, due to a lower Si content in AlSi7Mg, less Si is dissolved in the Al matrix when compared to AlSi10Mg. Consequently, less supersaturated Si will be able to nucleate in the primary Al cells to form intra-cellular Si precipitates. Therefore, the Si particle distribution in the primary Al cells of AlSi7Mg is much less dense when compared to AlSi10Mg. As such, the primary Al cells can still be observed in AlSi7Mg, while the microstructure of AlSi10Mg show a homogeneous fine distribution of Si particles with a small interspacing distance, and where the primary Al cells are no longer distinguishable. After SR2, nucleation of Si particles decays and the Si diffusion results in coarsening of the Si particles in the primary Al cells as well as at the cell boundaries. The coarsening of the Si particles results in an increase of the Si interspacing distance.

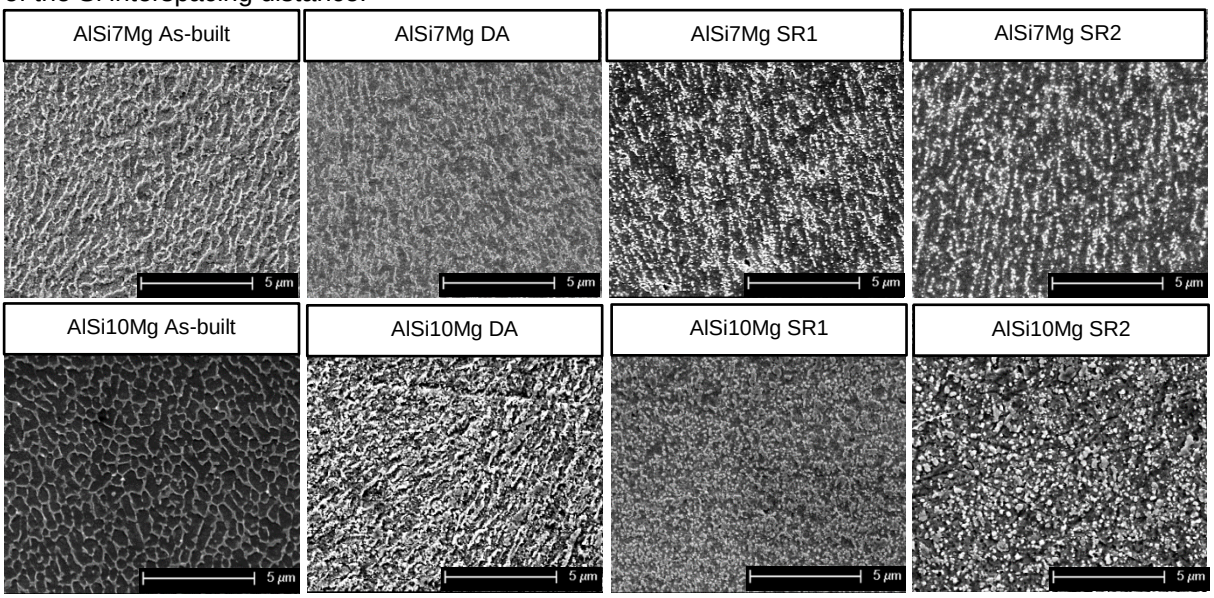

Figure 4: Microstructural evolution of LPBF AlSi7Mg (top row) and LPBF AlSi10Mg (bottom row) upon heat treatment.

III. Mechanical Properties and Residual Stresses

The evolution of the mechanical properties and the stress relief effectiveness of the heat treatments, are shown in Figure 5 a) and b), respectively. The mechanical properties of cast AlSi10Mg, heat treated according to T6, are included in Figure 5 a) as a reference and are based on the work of *Thijs et al.* [14]. The residual stress state was normalized to the as-printed condition for AlSi7Mg and AlSi10Mg respectively. Upon heat treatment, a similar evolution of the residual stress reduction can be observed for AlSi7Mg and AlSi10Mg. It must be noted that the used cantilever geometry mimics a worst case estimation, where 35-40% of the initial residual stresses remains in the cantilever after heat treatment. Yet, lower residual stresses are expected after heat treatment of industrial parts. Although the estimated residual stress state after heat treatment remains 35-40%, it is important to note that the residual stress effectiveness of the Direct Ageing and Stress Relief are almost equivalent.

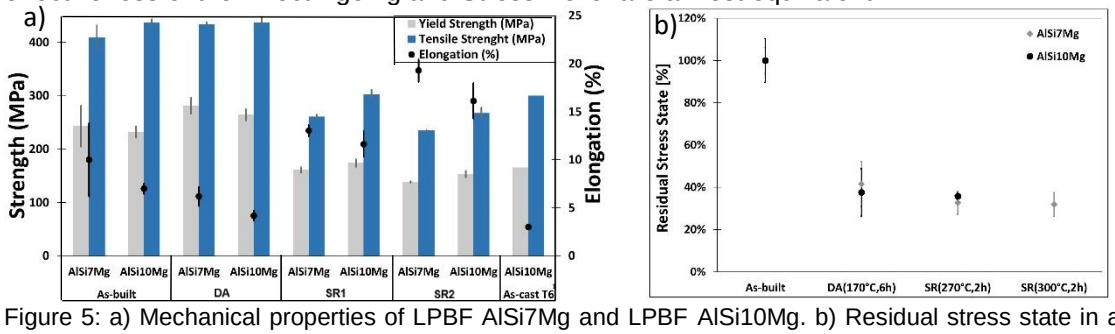

Figure 5: a) Mechanical properties of LPBF AlSi7Mg and LPBF AlSi10Mg. b) Residual stress state in as-printed condition and after heat treatment (right).

[1] The mechanical properties of AlSi10Mg as-cast T6 are based on the work of *Thijs et al.* [14]

In as-printed condition, similar high strength properties (UTS ~ 400MPa) are obtained for LPBF AlSi7Mg and LPBF AlSi10Mg. Due to the decreased Si content a less dense eutectic Si network is observed in LPBF AlSi7Mg, and thus a higher ductility is obtained for as-printed AlSi7Mg. For the DA, the strength is maintained while the ductility drops due to the fine precipitation of Si. As such, direct ageing is a suitable heat treatment for high strength applications. Both stress relief heat treatments induce a

significant drop in strength and a large increase in ductility, and obtains a similar residual stress state. The SR1 heat treatment attains a good balance between strength and ductility. The further drop in strength upon SR2 can be related to coarsening of the Si particles, thus increasing the Si interspacing distances, resulting in an easier dislocation movement during deformation. Despite the small temperature difference between SR1 and SR2, a major effect on the microstructure and mechanical properties of the Al-Si-Mg alloys is observed. Therefore, the large sensitivity of the mechanical properties on the temperature narrows the stress relief process window for LPBF AlSi7Mg and LPBF AlSi10Mg. It can be concluded that all conditions obtain superior mechanical properties compared to cast AlSi10Mg with subsequent T6 heat treatment.

CONCLUSION

Following conclusions are drawn from the current work:

- All studied conditions for LPBF AlSi7Mg and LPBF AlSi10Mg obtained superior mechanical properties compared to T6 heat treated cast AlSi10Mg, and marks the importance of tailoring heat treatments for LPBF Al-Si-Mg alloys. Thus, for LPBF Al-Si-Mg alloys, the solution annealing and quenching step from the T6 heat treatment have become redundant or even harmful for the mechanical properties.
- Through electrical resistivity measurements, the dissolved Si content in Al-Si-Mg alloys could be estimated in order to evaluate and monitor the degree of supersaturation for as-printed and heat treated conditions. Moreover, this technique may be useful for other LPBF precipitation hardenable alloys, to monitor the degree of supersaturation.
- The insights, gained from the evaluation of the thermo-physical characterization techniques (i.e. Electrical Resistivity, DSC, IET) allowed to optimize heat treatments for LPBF AlSi7Mg and AlSi10Mg and could be extrapolated to set up a methodology to design tailored heat treatments for other LPBF metals.
- For the stress relief heat treatment, a large sensitivity of the mechanical properties on the temperature narrows the heat treatment process window for LPBF AlSi7Mg and AlSi10Mg.

REFERENCES

[1] T. DebRoy *et al.*, “Additive manufacturing of metallic components – Process, structure and properties,” *Prog. Mater. Sci.*, vol. 92, pp. 112–224, 2018.

[2] L. Thijs, F. Verhaeghe, T. Craeghs, J. Van Humbeeck, and J. P. Kruth, “A study of the microstructural evolution during selective laser melting of Ti-6Al-4V,” *Acta Mater.*, vol. 58, no. 9, pp. 3303–3312, 2010.

[3] V. Cain, R. Knutsen, and J. Van Humbeeck, “Residual stress via the contour method in compact tension specimens produced via selective laser melting,” *Scr. Mater.*, vol. 87, pp. 29–32, 2014.

[4] P. C. Collins, D. A. Brice, P. Samimi, I. Ghamarian, and H. L. Fraser, “Microstructural Control of Additively Manufactured Metallic Materials,” *Annu. Rev. Mater. Res.*, vol. 46, no. 1, pp. 63–91, 2016.

[5] E. Brandl, U. Heckenberger, V. Holzinger, and D. Buchbinder, “Additive manufactured AlSi10Mg samples using Selective Laser Melting (SLM): Microstructure, high cycle fatigue, and fracture behavior,” *Mater. Des.*, vol. 34, pp. 159–169, 2012.

[6] N. T. Aboulkhair, I. Maskery, C. Tuck, I. Ashcroft, and N. M. Everitt, “The microstructure and mechanical properties of selectively laser melted AlSi10Mg: The effect of a conventional T6-like heat treatment,” *Mater. Sci. Eng. A*, vol. 667, pp. 139–146, 2016.

[7] F. Stadler, H. Antrekowitsch, W. Fragner, H. Kaufmann, E. R. Pinatel, and P. J. Uggowitzer, “The effect of main alloying elements on the physical properties of Al-Si foundry alloys,” *Mater. Sci. Eng. A*, vol. 560, pp. 481–491, 2013.

[8] M. Tang, “Inclusions, Porosity, and Fatigue of AlSi10Mg Parts Produced by Selective Laser Melting,” *Int. J. Fatigue*, vol. 94, no. April, p. 184, 2017.

[9] S. Marola *et al.*, “A comparison of Selective Laser Melting with bulk rapid solidification of AlSi10Mg alloy,” *J. Alloys Compd.*, vol. 742, pp. 271–279, 2018.

[10] J. Fiocchi, A. Tuissi, P. Bassani, and C. A. Biffi, “Low temperature annealing dedicated to AlSi10Mg selective laser melting products,” *J. Alloys Compd.*, vol. 695, pp. 3402–3409, 2017.

[11] P. Wei *et al.*, “The AlSi10Mg samples produced by selective laser melting: single track, densification, microstructure and mechanical behavior,” *Appl. Surf. Sci.*, vol. 408, pp. 38–50, 2017.

[12] W. Li *et al.*, “Effect of heat treatment on AlSi10Mg alloy fabricated by selective laser melting: Microstructure evolution, mechanical properties and fracture mechanism,” *Mater. Sci. Eng. A*, vol. 663, pp. 116–125, 2016.

[13] N. Takata, H. Kodaira, K. Sekizawa, A. Suzuki, and M. Kobashi, “Change in microstructure of

selectively laser melted AlSi10Mg alloy with heat treatments," *Mater. Sci. Eng. A*, vol. 704, no. May, pp. 218–228, 2017.

[14] L. Thijs, *Microstructure and texture of metal parts produced by Selective Laser Melting*, vol. PhD, no. February. 2014.